

University of Groningen

Fluorescence imaging to localize head and neck squamous cell carcinoma for enhanced pathological assessment

Warram, Jason M.; de Boer, Esther; van Dam, Gooitzen M.; Moore, Lindsay S.; Bevans, Stephanie L.; Walsh, Erika M.; Young, Erik S.; Carroll, William R.; Stevens, Todd M.; Rosenthal, Eben L.

Published in:

Journal of pathology clinical research

DOI:

[10.1002/cjp2.40](https://doi.org/10.1002/cjp2.40)

IMPORTANT NOTE: You are advised to consult the publisher's version (publisher's PDF) if you wish to cite from it. Please check the document version below.

Document Version

Publisher's PDF, also known as Version of record

Publication date:

2016

[Link to publication in University of Groningen/UMCG research database](#)

Citation for published version (APA):

Warram, J. M., de Boer, E., van Dam, G. M., Moore, L. S., Bevans, S. L., Walsh, E. M., Young, E. S., Carroll, W. R., Stevens, T. M., & Rosenthal, E. L. (2016). Fluorescence imaging to localize head and neck squamous cell carcinoma for enhanced pathological assessment. *Journal of pathology clinical research*, 2(2), 104-112. <https://doi.org/10.1002/cjp2.40>

Copyright

Other than for strictly personal use, it is not permitted to download or to forward/distribute the text or part of it without the consent of the author(s) and/or copyright holder(s), unless the work is under an open content license (like Creative Commons).

The publication may also be distributed here under the terms of Article 25fa of the Dutch Copyright Act, indicated by the "Taverne" license. More information can be found on the University of Groningen website: <https://www.rug.nl/library/open-access/self-archiving-pure/taverne-amendment>.

Take-down policy

If you believe that this document breaches copyright please contact us providing details, and we will remove access to the work immediately and investigate your claim.

Fluorescence imaging to localize head and neck squamous cell carcinoma for enhanced pathological assessment

Jason M Warram,¹ Esther de Boer,^{1,2} Gooitzen M van Dam,² Lindsay S Moore,¹ Stephanie L Bevans,³ Erika M Walsh,¹ Erik S Young,⁴ William R Carroll,¹ Todd M Stevens⁴ and Eben L Rosenthal^{5*}

¹ Department of Otolaryngology, University of Alabama at Birmingham, Birmingham, AL

² Department of Surgery, Nuclear Medicine and Molecular Imaging, and Intensive Care, University Medical Center Groningen, University of Groningen, The Netherlands

³ Department of Medicine, School of Medicine, University of Alabama at Birmingham, Birmingham, AL 35233

⁴ Department of Pathology, Division of Anatomic Pathology, University of Alabama at Birmingham, Birmingham, AL 35233

⁵ Department of Otolaryngology, Stanford University, Stanford, CA 94305

*Correspondence to: Eben L. Rosenthal, Department of Otolaryngology, Stanford University, 875 Blake Wilbur Drive Suite CC-2212, Stanford CA 94305. e-mail: elr@stanford.edu.

Abstract

Accurately identifying close or positive margins in real-time permits re-excision during surgical procedures. Intraoperative assessment of margins via gross examination and frozen section is a widely used tool to assist the surgeon in achieving complete resection. While this methodology permits diagnosis of freshly resected tissue, the process is fraught with misinterpretation and sampling errors. During fluorescence-guided surgery, an exogenous fluorescent agent specific for the target disease is imaged in order to navigate the surgical excision. As this technique quickly advances into the clinic, we hypothesize that the disease-specific fluorescence inherently contained within the resected tissues can be used to guide histopathological assessment. To evaluate the feasibility of fluorescence-guided pathology, we evaluated head and neck squamous cell carcinoma tumour specimens and margins resected from animals and patients after systemic injection of cetuximab-IRDye800CW. In a preclinical model of luciferase-positive tumour resection using bioluminescence as the gold standard, fluorescence assessment determined by closed-field fluorescence imaging of fresh resected margins accurately predicted the presence of disease in 33/39 positive margins yielding an overall sensitivity of 85%, specificity of 95%, positive predictive value (PPV) of 94%, and a negative predictive value (NPV) of 87%, which was superior to both surgical assessment (54%, 61%, 57%, and 58%) and pathological assessment (49%, 95%, 91%, and 66%), respectively. When the power of the technique was evaluated using human-derived tumour tissues, as little as 0.5mg (1mm³) of tumour tissue was identified (tumour-to-background-ratio:5.2). When the sensitivity/specificity of fluorescence-guided pathology was determined using traditional histological assessment as the gold standard in human tissues obtained during fluorescence-guided surgery, the technique was highly accurate with a sensitivity of 91%, specificity of 85%, PPV of 81%, and NPV of 93% for 90 human-derived samples. This approach can be used as a companion to the pathologist, eliminating confounding factors while impacting surgical intervention and patient management.

Keywords: surgical pathology; surgical margins; frozen section; fluorescence imaging

Received 7 December 2015; accepted 16 January 2016

The authors have declared no conflicts of interest.

Introduction

Currently, surgeons and pathologists lack the adequate and reliable intraoperative tools to consistently discriminate tumour and normal tissue in real-time. This has resulted in high rates of positive or close margins in head and neck squamous cell carcinoma (HNSCC), which is associated with high local rates of recurrence [1]. Positive margins are

associated with a 22% local recurrence rate, compared to 3.9% local recurrences in patients with tumour-free margins [2]. Moreover, involved surgical margins increase the risk of death at 5 years by 90%, indicating that surgical margin status remains a primary predictor for survival and local recurrence [3]. Nevertheless, in current clinical practice, tumour positive margins are found in up to 40% of patients on

histopathological review [4,5], for which there is clear need for improvement.

Currently, intraoperative frozen section analysis of margins is a widely used tool to assist the surgeon in achieving complete tumour resection. While this methodology permits rapid turnaround for diagnosis of freshly resected tissue, the process is not real-time and there is a poor correlation of frozen and permanent margin status in HNSCC. In a recent study, discordance between frozen and permanent margins was identified in 20% of cases [6]. More specifically, the false-negative rate for poorly differentiated carcinoma, lymphovascular invasion, and perivascular invasion was 14%, 36%, and 26%, respectively. In addition to misinterpretation and specimen under-sampling, these histopathological features are associated with a higher rate of discrepancy between frozen and permanent assessment [7–9]. Considering HNSCC has the highest rate of intraoperative consultations [10], investigating alternative more accurate methodologies for margin assessment is of greatest relevance to this tumour type. However, discordant final diagnosis affects patient management in all tumour types, both at the surgical intervention and long-term treatment stages.

In response to limited improvement of survival rates in surgical oncology, there have been several landmark clinical trials demonstrating that cancer can be accurately identified in real-time using fluorescence-guided surgical techniques [11–13]. As a result, the field of fluorescence-guided surgery has grown significantly and additional clinical trials are underway to evaluate a range of fluorescently labeled, cancer-specific contrast agents to guide surgical ablation in multiple cancer types. The advantage of fluorescence-guided surgery is that it localizes diseased tissue that would otherwise remain undetected during traditional standard of care. For example, in phase III clinical trials, oral administration of 5-aminolevulinic acid (5-ALA) was shown to improve progression-free survival [12,14]. Recently, our group conducted a phase I dose-escalation study in twelve patients using cetuximab-IRDye800CW in squamous cell carcinoma arising in the head and neck (clinicaltrials.gov identifier: NCT01987375). During the intraoperative imaging, disease-specific fluorescence generated high levels of contrast (tumour-to-background ratios average of 5.2) to delineate cancer from normal tissues in the operative field [11,15]. During this clinical trial, it became apparent that identification of disease by fluorescence imaging of the surgical specimen had significant advantages for the pathologist, such as identifying areas in the gross specimen where the margins are likely to be close or positive, thus allowing efficient and focused tumour sampling

for histological sections. Considering the challenges of appropriate sampling and time required for intraoperative consultation, we hypothesize that a cancer-specific fluorescent contrast agent, systemically injected prior to the surgical procedure, could be used to guide pathological assessment of close or positive margins. Imaging the primary specimen in the frozen section room prior to sampling the tumour periphery may help guide the pathologist to identify suspicious areas for frozen section, which, if positive for carcinoma, would allow the surgeon to re-excite this area at the time of the original procedure. As a proof of concept, we set up a translational experimental approach in which we evaluated the technique in a preclinical model of cancer where bioluminescence imaging was utilized as the gold standard for detection of microscopic disease. To evaluate clinical feasibility of this fluorescence-guided pathology approach, we evaluated HNSCC tumour specimens resected from animals and humans after systemic injection of cetuximab-IRDye800CW. To determine the sensitivity and specificity of fluorescence-guided pathology, we compared the approach to traditional histological assessment using human tissues obtained during a clinical trial of fluorescence-guided surgery in HNSCC.

Methods

Cetuximab-IRDye800CW conjugation

Conjugation of cetuximab to IRDye800CW (excitation: 778 nm, emission: 798 nm) was performed under cGMP conditions as previously reported [16]. Briefly, cetuximab® (ImClone LLC, subsidiary of Eli Lilly and Company, Branchburg, NJ) was concentrated and pH adjusted by buffer exchange to a 10 mg/ml solution in 50 mM potassium phosphate, pH 8.5. IRDye800CW NHS ester (LI-COR Biosciences, Lincoln, NE) was conjugated to cetuximab for 2 hrs at 20°C in the dark, at a molar ratio of 2.3:1. After column filtration to remove unconjugated dye and exchange buffer to phosphate buffered saline (PBS), pH 7, the final protein concentration adjusted to 2 mg/ml, the product was sterilized by filtration and placed into single use vials and stored at 4°C until used.

Cell line and animal models

The human head and neck squamous cell carcinoma cell line SCC1 was obtained from the University of Michigan and maintained in Dulbecco's Modified Eagle's Medium (DMEM) with 10% fetal bovine

serum and 2.6 mM L-glutamine. Cells were cultured at 37°C and 5% CO₂, passaged at 70 to 90% confluence, and harvested with 0.05% trypsin/0.53 mM EDTA. Cell lines were genetically modified with a luciferase-expressing construct (pCMV pGL3 Luciferase, Addgene, Cambridge, MA). Athymic female nude mice (aged 6–8 weeks) were obtained from Frederick Cancer Research (Frederick, MD). For subcutaneous inoculation, 2×10^6 SCC1-luc cells were bilaterally implanted in the right and left hind flank of each mouse. Institutional Animal Care and Use Committee (IACUC) at the University of Alabama at Birmingham approved all animal protocols (APN 130908793; 140310064).

In vivo margin study

Three weeks post implant (average tumour size: 188.3 ± 15 mm³), athymic nude mice ($n = 10$) bearing bilateral subcutaneous flank tumours received 225 µg (62.5 mg/m², one-quarter cetuximab therapeutic dose) of cetuximab-IRDye800CW (excitation: 778 nm, emission: 798 nm) intravenously via tail vein. Five days post injection, mice were sacrificed, tumours resected and four margins (1 cm × 0.5 cm × 0.5 cm, each) collected from each wound bed (80 margins total). For the surgeon's assessment, an otolaryngology surgery resident (EMW) visually assessed the resected margins to determine the presence of tumour. Fluorescence imaging of each margin was performed using the Pearl Impulse (LI-COR Biosciences, Lincoln, NE). For the imaging, specimens were placed in the imaging tray and acquisitions were performed using onboard instrument software at the 800 nm channel (emission filter 810–830 nm), 85 µm resolution, and 0 focus position. Fluorescence imaging was performed on both sides of each specimen. After addition of a luciferase assay agent (E1500, Promega, Madison, WI) bioluminescence imaging (BLI, IVIS-100, Caliper Life Sciences, Waltham, MA) was performed on each resected margin using the 500–570 nm emission filter setting. The term bioluminescence describes the emission of light generated as a byproduct of the enzymatic reaction between firefly luciferase enzyme and a substrate, luciferin. Margins were fixed in formalin and processed into paraffin blocks; 5 µm tissue sections were then cut (2) 100 µm apart, placed on glass slides, and stained with haematoxylin & eosin (H&E). A University of Alabama at Birmingham (UAB) board-certified pathologist (TMS) was blinded to the bioluminescence data and fluorescence grading and examined the slides by light microscopy and H&E staining to determine if tumour cells were present or

absent in the margins by conventional analysis. The blinded fluorescence assessment was performed using onboard instrument software (ImageStudio, LI-COR Biosciences). For the assessment, the threshold was uniquely adjusted for each sample to reveal heterogeneity in fluorescence intensity within each sample, as previously described [17–19]. Areas of high signal relative to the surrounding tissue were considered positive. Margins were given a binary assignment (\pm) determined by the presence or absence of tumour by each test. The diagnostic accuracy of the surgeon's assessment, fluorescence prediction, and conventional histological evaluation using H&E stain was compared to the bioluminescence (gold standard) results to calculate the sensitivity, specificity, positive predictive value (PPV), and negative predictive value (NPV).

In vitro margin study

To produce surrogate margins using a xenograft mouse model, athymic nude mice ($n = 5$) bearing subcutaneous flank tumours (SCC1) received 225 µg (62.5 mg/m², one-quarter cetuximab therapeutic dose) of cetuximab-IRDye800CW intravenously via tail vein. Five days post injection, mice were sacrificed, tumours resected, grossly sectioned and weighed. Muscle (2 cm × 1 cm × 0.5 cm) was excised from the contralateral flank to serve as normal tissue. Serially sectioned tumour fragments ranging from 5 mg to 0.5 mg in size were then placed onto the excised muscle bed and imaged using the Pearl Impulse. For evaluation using clinically obtained tissue, human tissue obtained during a clinical trial evaluating the safety of cetuximab-IRDye800CW in patients undergoing surgical intervention for squamous cell carcinoma arising in the head and neck (clinicaltrials.gov identifier#NCT01987375) were examined. Three to 4 days prior to surgery, patients received intravenous infusion of 62.5 mg/m² cetuximab-IRDye800CW. Tumour tissue excised from the bulk tumour by the ablative surgeon was serially sectioned and weighed to produce sections ranging from 5 mg to 0.5 mg. These sections were then placed on patient-matched muscle and imaged using the Pearl Impulse. Informed consent was obtained from participating patients and the UAB Institutional Review Board previously approved the research.

Surrogate margin study

During a clinical trial evaluating the safety of cetuximab-IRDye800CW in patients undergoing

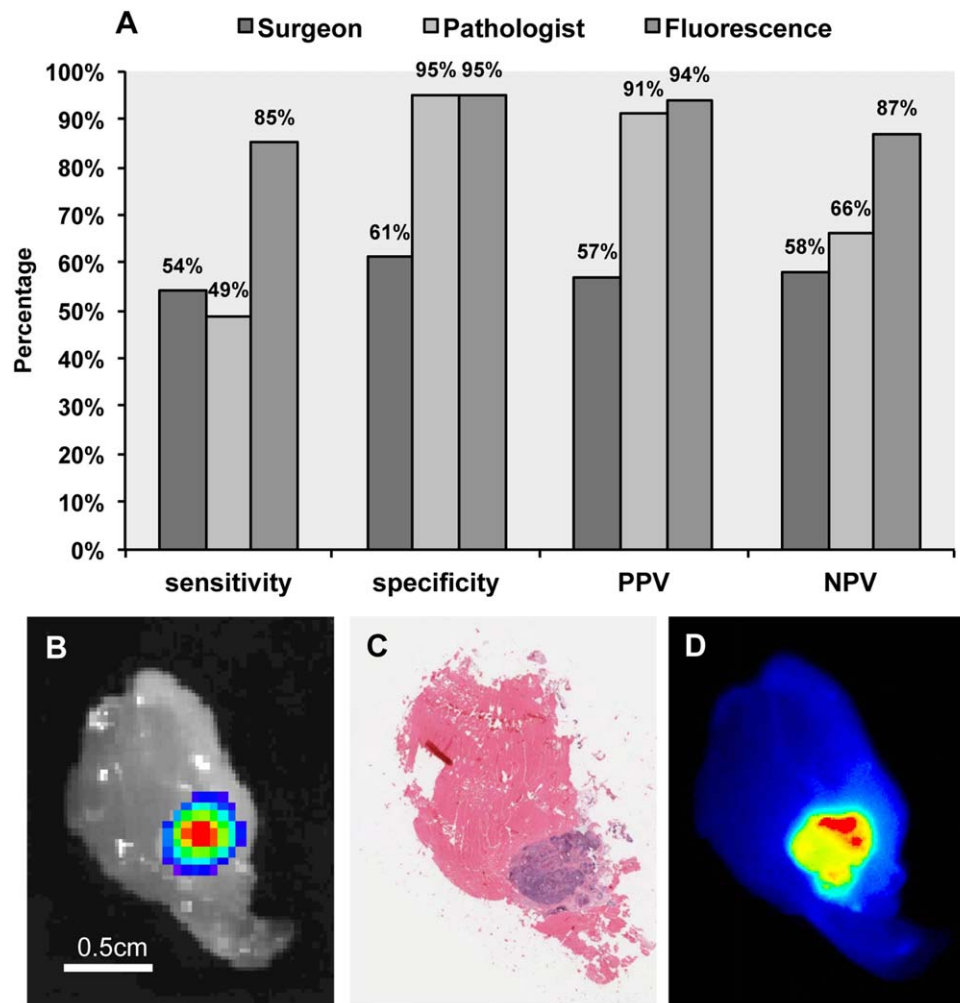


Figure 1. Fluorescence localization of disease is compared to histopathological assessment and surgeon assessment using luciferase imaging as gold standard. (A) Sensitivity, specificity, positive predictive value (PPV), and negative predictive value (NPV) are shown for surgeon, pathologist, and fluorescence assessment of tumour wound-bed margins compared to bioluminescence, which served as the gold standard. Representative images are shown of the margins assessed for (B) bioluminescence, (C) haematoxylin and eosin staining, and (D) matching fluorescence acquisition.

surgical intervention for squamous cell carcinoma arising in the head and neck (clinicaltrials.gov identifier#NCT01987375), a total of 45 punch biopsies (1 cm × 4 mm) were collected by the ablative surgeon from resected primary tumour specimens excised from three patients ($n = 15$ each). Biopsies were then bisected to produce 90 tissue samples, imaged with Pearl Impulse, and histologically processed. After H&E staining, UAB pathologists examined the slides by light microscopy to determine if tumour cells were present or absent in the margins by conventional analysis. Each specimen was subdivided into quarters and a binary assignment given to each quarter based on the presence or absence of cancer by histological analysis and fluorescence

assessment. The result of fluorescence prediction using fluorescence imaging was compared to conventional histological evaluation using H&E staining (gold standard) to calculate the sensitivity, specificity, PPV, and NPV. Informed consent was obtained from participating patients and the UAB Institutional Review Board previously approved the research.

Fluorescence microscopy

Unstained slide-mounted sections of patient-derived tissues were imaged (400×) using a fluorescence microscope (Leica DMI6000B) equipped with a DFC365FX near-infrared camera and an XCite200 light source and onboard LAS X software. After

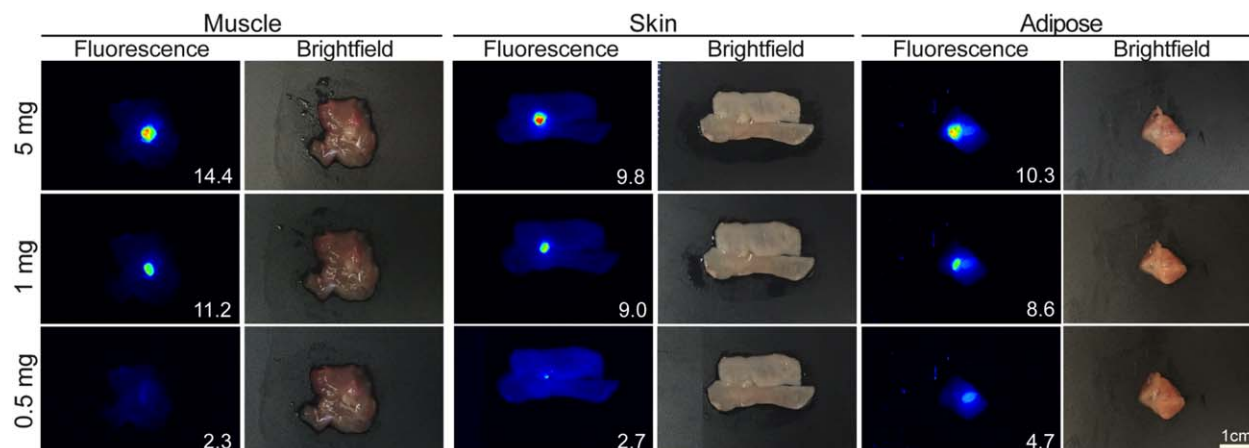


Figure 2. Minimum disease detectable in mouse tissues. Representative fluorescence and brightfield images are shown for 5 mg, 1 mg, and 0.5 mg tumour fragments on a bed of muscle, skin, or adipose tissue from mice infused with cetuximab-IRDye800CW 5 days prior to tumour resection. Inset values represent tumour to background ratios for the respective tissue.

fluorescence acquisition, slides were H&E stained and matching brightfield images (400×) were acquired using an Olympus IX70 equipped with a DP72, 12.8 megapixel cooled digital colour camera.

Results

Fluorescence assessment accurately predicts the presence of residual disease in an animal model of surgical margins

To evaluate the feasibility of fluorescence-guided pathology to detect subclinical disease, an animal model of diseased margins was used to compare fluorescence assessment to conventional assessment using bioluminescence, *in lieu* of histology as the gold standard. For the experiment, 80 margins were collected from post-resection wound beds of 20 luciferase positive SCC1-luc tumours resected from the subcutaneous flank of mice that received a systemic administration of cetuximab-IRDye800CW. As shown in Figure 1A, the fluorescence assessment determined by closed-field fluorescence imaging (Pearl) of fresh resected margins accurately predicted the presence of disease in 33 of 39 positive margins yielding an overall sensitivity of 85%, specificity of 95%, PPV of 94%, and NPV of 87%. More importantly, fluorescence successfully predicted the absence of disease in 39 out of 41 negative margins, as determined by bioluminescence imaging. For the histological assessment, all 80 tissue margins were sectioned (5 µm full-face thickness), slide-mounted for H&E staining (two per margin, cut 100 µm apart) and then examined by a board-certified pathologist

and a binary (\pm) value was assigned for each margin based on the presence of tumour. During the assessment, the pathologist accurately predicted the presence of tumour in 21 out of 39 disease containing margins (TMS) yielding an overall sensitivity of 49%, specificity of 95%, PPV of 91%, and a NPV of 66%. However, similarly to the fluorescence assessment group, the pathologist correctly predicted the absence of disease in 39 out of 41 negative margins. The surgeon assessment was also evaluated and found to have a sensitivity of 54%, specificity of 61%, PPV of 57%, and NPV of 58%. To demonstrate the disease localization between the various modalities evaluated, a bioluminescence image (Figure 1B), matching H&E stained histological section (Figure 1C), and fluorescence acquisition (Figure 1D) of a representative margin containing residual disease are shown.

Subclinical residual tumour was successfully localized using fluorescence imaging in a model of positive surgical margins using mouse tissues

To evaluate the potential of fluorescence-guided pathology to localize subclinical tumour during margin assessment, human xenograft tumours were grown subcutaneously in mice that received a systemic injection of cetuximab-IRDye800CW. Tumours were resected (day 5 post cetuximab-IRDye800CW injection) and serially sectioned to produce 5 mg, 1 mg, and 0.5 mg pieces of tumour. To create surrogate margins of residual disease, muscle, skin, and adipose tissue were excised and used as normal tissue backgrounds. The ability to discern between tumour and normal tissue was quantified using tumour-to-

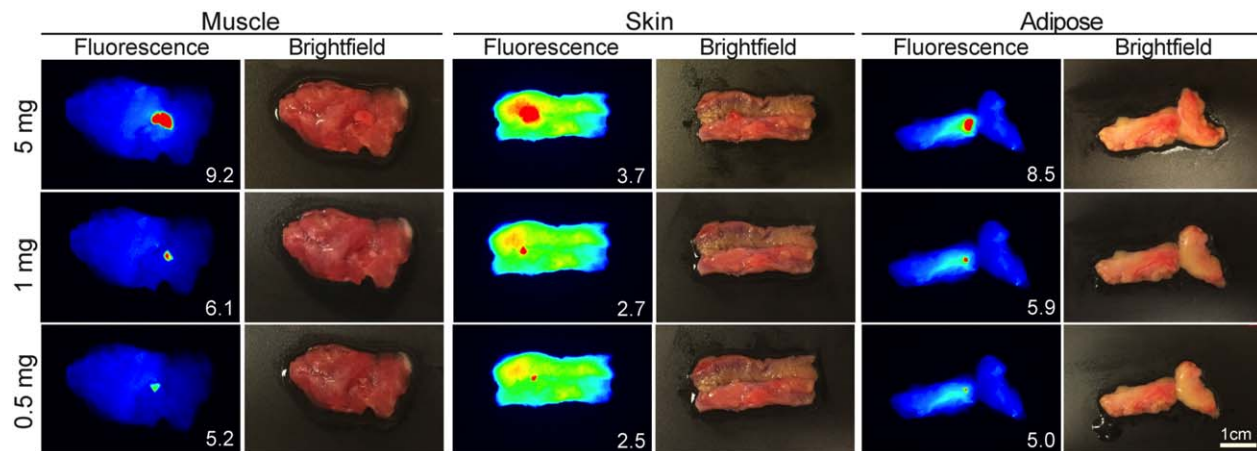


Figure 3. Minimum disease detectable in human tissues. Representative fluorescence and brightfield images are shown for 5 mg, 1 mg, and 0.5 mg human-derived tumour fragments on a bed of patient-matched muscle, skin, or adipose tissue from a patient infused with cetuximab-IRDye800CW 3 days prior to tumour resection. Inset values represent tumour to background ratios for the respective tissue.

background ratios (TBR) of mean fluorescence intensity. When each tumour tissue fragment was serially placed on a respective background tissue, the tumour was successfully fluorescently localized (Figure 2) with TBRs ranging between 14.4 for the muscle background and 9.8 for the skin background using the 5 mg tumour fragment. When evaluating the sensitivity of the approach to detect subclinical disease using the 0.5 mg tumour fragment, TBR values ranged from 4.7 to 2.3 when adipose and muscle tissue, respectively, were tested.

Assessment of subclinical disease using fluorescence imaging in a model of positive surgical margins using human tissues

To demonstrate the translatability of the fluorescence-guided pathology approach, resected tumour tissue (squamous cell carcinoma) from a clinical trial patient, who received cetuximab-IRDye800CW (62.5 mg/m² dose) 3 days prior to undergoing a total glossectomy, was serially sectioned to produce 5 mg, 1 mg, and 0.5 mg tumour fragments. Patient-matched tissues (muscle, skin, and adipose) were used as background and individual tumour fragments were serially placed on each background tissue type to mimic surgical margins. As shown in Figure 3, the human tumour fragments were successfully visualized (TBR > 1) at each tumour fragment weight and tissue background. For the 5 mg fragment, TBRs ranged between 9.2 for the muscle background and 3.7 for the skin background. Likewise, the subclinical 0.5 mg fragment (1 mm³) exhibited TBR values ranging between 5.2 for the

muscle background and 2.5 for the skin background. Matching brightfield images are also shown to demonstrate the difficulty in localizing the subclinical diseased tissue under white light conditions.

Fluorescence-guided pathology is highly sensitive when compared to traditional histological methods

To compare the reliability of fluorescence-guided pathology to the current standard of care, 4 mm tissue punch biopsies ($n = 45$) collected from resected primary tumour specimens ($n = 3$, Figure 4A, B) from patients who received cetuximab-IRDye800CW (62.5 mg/m² dose) 3 days prior to undergoing ablative surgery were bisected and imaged with the closed-field fluorescence imaging device prior to formalin fixation and paraffin embedding. Images obtained of the whole tissue samples were subdivided into quarters and a binary \pm assessment was assigned to each quarter based on the presence of disease as determined by fluorescence assessment (Figure 4C). The samples were then processed for histology and the histological assessment of each biopsy quarter was performed using H&E stained sections of each punch biopsy by a board-certified pathologist in a blinded fashion (Figure 4D). Biopsies were bisected to reduce potential sample error during the histological processing. A fluorescence image of a representative primary specimen annotated with the locations of punch biopsy samples is shown in Figure 4B. Using histological assessment as the gold standard, fluorescence assessment

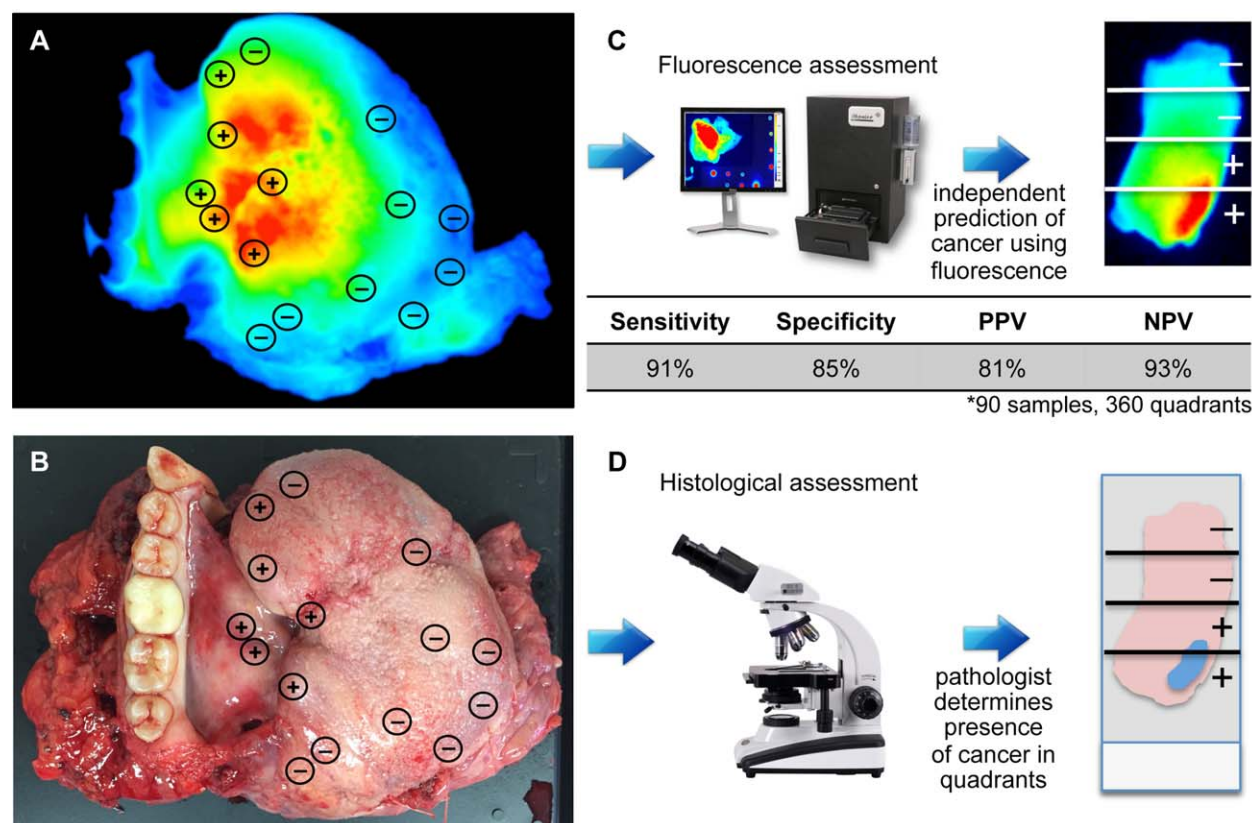


Figure 4. Fluorescence assessment of patient-derived surrogate margins. Fluorescence (A) and brightfield (B) images are shown of representative resected primary tumour specimens from a patient who received cetuximab-IRDye800CW 3 days prior to undergoing ablative surgery. Areas sampled with 4 mm punch biopsy are annotated with histological assessment (\pm). Specimens were subdivided into quarters and a binary \pm assessment was assigned to each quarter based on the presence of disease as determined independently by (C) fluorescence assessment of whole tissue and (D) histological assessment of slide-mounted, H&E-stained sections. Using histological assessment as the gold standard, results from fluorescence assessment were correlated with the gold standard to determine sensitivity, specificity, positive predictive value (PPV), and negative predictive value (NPV).

accurately predicted the presence of disease in 137 out of 151 tumour-containing quarters to yield an overall sensitivity of 91%, specificity of 85%, PPV of 81%, and NPV of 93% for 90 punch biopsy samples and 360 quarters.

Fluorescence microscopy confirmed disease-specific fluorescence intensity

To confirm the disease-specific nature of the fluorescence intensity observed in the human tissues tested, fluorescence microscopy was performed. Figure 5A shows an H&E stained section of a primary tumour specimen of oral (tongue) squamous cell carcinoma from a patient who received cetuximab-IRDye800CW (62.5 mg/m² dose) 3 days prior to undergoing ablative surgery. A board-certified pathologist annotated the image (green line) to outline the cancer-containing areas, which correlated precisely

with the fluorescence microscopy image shown in Figure 5B. A nuclear stain image (DAPI) is also shown in Figure 5C.

Discussion

In this proof-of-principle study, we evaluated the potential of disease-specific fluorescence to positively identify subclinical tumour within the post-resection wound bed and within surgical margins. To recreate surgical margins for testing, surrogate margins were generated using a translational experimental design with both mouse and human tissue. The ability of fluorescence assessment to localize disease in these margins was shown to be highly sensitive and specific with a NPV of 87%, which was superior to both surgical assessment (58%) and pathological assessment (66%), when using bioluminescence imaging as

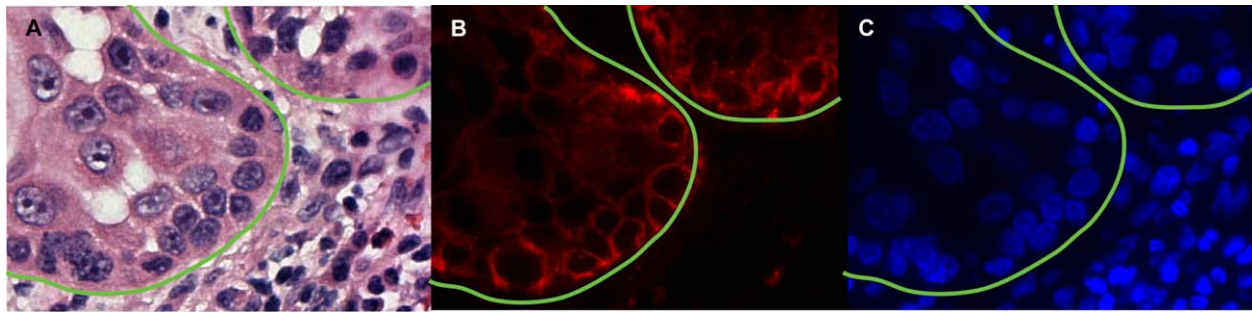


Figure 5. Fluorescence microscopy of cetuximab-IRDye800CW infused patient-derived tumour. (A) Representative H&E microscopy image (400×) with pathology-positive areas of tumour outlined in green. (B) Fluorescence microscopy (400×) acquired using custom IRDye800CW filter sets is shown with correlating (C) DAPI nuclear stain.

the gold standard. Using both mouse and human tissues, we found that as little as 0.5 mg of human tumour tissue was identified (TBR: 5.2) when patient-matched muscle was used as background. In the clinical setting, a 0.5 mg tumour is equivalent to less than 10^5 cells with a tumour diameter of ~ 1 mm [20]. This would be considered subclinical disease, since it is smaller than is currently detectable. When the fluorescence-guided pathology technique was used to assess subclinical disease fragments (surrogate margins) collected from primary tumour specimens from patients who received cetuximab-IRDye800CW prior to undergoing ablative surgery, the approach was shown to be highly effective to localize cancer-containing quarters with a NPV of 93%. Importantly, fluorescence microscopy of the surrogate margins demonstrated the cancer-specific nature of the fluorescence, which confirmed that the fluorescence signal correlated with tumour-containing areas.

Although the limit of fluorescence detection was found to be approximately 0.5 mg of tumour, it far exceeded current detection modalities. The fluorescence assessment (sensitivity: 85%) strongly outperformed the surgeon (sensitivity: 54%) and the pathologist (sensitivity: 49%) at identifying positive margins (Figure 1). There is a possibility that sampling error during tissue block sectioning (unsectioned tumour present deeper in the tissue block) played a role in the low sensitivity of the pathology assessment. However, when the ability of pathological assessment to correctly identify negative margins was evaluated, fluorescence assessment (specificity: 95%) and pathology assessment performed identically, while the surgeon assessment remained low (specificity: 61%). This comparison illustrates the success of pathological assessment when tumour-containing tissue is captured on the slide for analysis. However, if sampling error occurs and the tumour

region is not identified for sectioning, the margin will be erroneously assessed as negative. Using fluorescence assessment, the pathologist or surgeon is able to perform directed or fluorescent-guided sampling which may limit the false negative result from sampling error, particularly in larger specimens. For example, if initial levels from a tissue block containing a tissue section from a fluorescently “hot” area are negative for tumour, the pathologist would be prompted to obtain deeper levels from this block where tumour is likely hiding, thereby turning a potentially false negative margin into a true positive margin. This underlines the benefit of fluorescence to localize suspicious areas of the margin for more accurate histopathological assessment.

For exogenously administered fluorescence imaging agents, target-specific differences within tissues may limit the widespread application of fluorescence-guided pathology. During the study, epidermal growth factor receptor (EGFR), which served as the targeted epitope of cetuximab-IRDye800CW, in the skin led to a 50% reduction in TBRs when patient-matched skin was used as the background. Likewise, restraints in fluorescence penetration may limit the application when larger margins (>1 cm) are assessed. Lower wavelength dyes are limited in sensitivity due to the high attenuation and scattering effects that are associated with these dyes. For the current study, the near infrared IRDye800CW was utilized due to the superior penetration (1 cm) provided by this dye [21]. As the fluorescence-guided pathology approach is developed, it will be critical for the pathologist to be aware of the off-target accumulation and the fluorescence potential of the imaging agent.

This report provides evidence that tumour-specific fluorescence can be used by the surgeon or pathologist to guide sampling for frozen sections, but does not replace the need for histological diagnosis. Although fluorescence guidance may be better than

conventional sampling techniques, which include inspection and palpation, it does not allow for histopathological analysis of tissue to confirm margins on frozen sections. With the substantial increase in clinical trials evaluating fluorescence-guided surgery, it is not difficult to imagine the future of surgical oncology incorporating such technology. These tools serve to enhance the surgeon's ability to successfully identify and resect tumour while eliminating over-resection to retain normal function. Fluorescence-guided pathology can then be easily implemented into the clinical care workflow and used in adjunct to fluorescence-guided surgery to help guide the pathologist when assessing margins for both intraoperative assessment and staging.

Acknowledgements

Work was supported by grants from NIH (R21CA182953, R21CA17917, T32CA091078), UAB Comprehensive Cancer Center, and Robert Armstrong Research Fund. Institutional equipment loans from LICOR and Novadaq also supported this research. In addition to institutional funding provided by UAB and the University Medical Center Groningen, this work was further supported by the Stichting Prof. Michaël-van Vloten fonds. The authors thank Dr. Neel Patel, Ms. Yolanda Hartman, and Ms. Lisa Clemons for their assistance in this study.

Author Contributions

JMW and ELR carried out data analysis, manuscript writing, study design, data collection, data interpretation; EdB, GVD, LSM, and TMS performed the data analysis, figures, data collection, data interpretation; LB and ESY carried out the study design, data analysis; EMW carried out the data collection and manuscript writing; WRC carried out data collection and study design.

References

1. Nguyen TH, Ho DQ. Nonmelanoma skin cancer. *Curr Treat Options Oncol* 2002; **3**: 193–203.
2. Slootweg PJ, Hordijk GJ, Schade Y, et al. Treatment failure and margin status in head and neck cancer. A critical view on the potential value of molecular pathology. *Oral Oncol* 2002; **38**: 500–503.
3. Binahmed A, Nason RW, Abdoh AA. The clinical significance of the positive surgical margin in oral cancer. *Oral Oncol* 2007; **43**: 780–784.
4. McMahon J, O'Brien CJ, Pathak I, et al. Influence of condition of surgical margins on local recurrence and disease-specific survival in oral and oropharyngeal cancer. *Br J Oral Maxillofac Surg* 2003; **41**: 224–231.
5. Woolgar JA, Triantafyllou A. A histopathological appraisal of surgical margins in oral and oropharyngeal cancer resection specimens. *Oral Oncol* 2005; **41**: 1034–1043.
6. Chambers KJ, Kraft S, Emerick K. Evaluation of frozen section margins in high-risk cutaneous squamous cell carcinomas of the head and neck. *Laryngoscope* 2015; **125**: 636–639.
7. Golouh R, Bracko M. Accuracy of frozen section diagnosis in soft tissue tumors. *Mod Pathol* 1990; **3**: 729–733.
8. Terpe HJ, Muller W, Liese A, et al. [Frozen section telepathology in the clinical routine of a breast cancer center]. *Pathologe* 2003; **24**: 150–153.
9. Weinberg E, Cox C, Dupont E, et al. Local recurrence in lumpectomy patients after imprint cytology margin evaluation. *Am J Surg* 2004; **188**: 349–354.
10. Mahe E, Ara S, Bishara M, et al. Intraoperative pathology consultation: error, cause and impact. *Can J Surg* 2013; **56**: E13–E18.
11. Rosenthal EL, Warram JM, de Boer E, et al. Safety and tumor specificity of Cetuximab-IRDye800 for surgical navigation in head and neck cancer. *Clin Cancer Res* 2015; **21**: 3658–3666.
12. Stummer W, Pichlmeier U, Meinel T, et al. Fluorescence-guided surgery with 5-aminolevulinic acid for resection of malignant glioma: a randomised controlled multicentre phase III trial. *Lancet Oncol* 2006; **7**: 392–401.
13. van Dam GM, Themelis G, Crane LM, et al. Intraoperative tumor-specific fluorescence imaging in ovarian cancer by folate receptor- α targeting: first in-human results. *Nat Med* 2011; **17**: 1315–1319.
14. Aldave G, Tejada S, Pay E, et al. Prognostic value of residual fluorescent tissue in glioblastoma patients after gross total resection in 5-aminolevulinic acid-guided surgery. *Neurosurgery* 2013; **72**: 915–920; discussion 920–911.
15. de Boer E, Warram JM, Tucker MD, et al. In vivo fluorescence immunohistochemistry: localization of fluorescently labeled cetuximab in squamous cell carcinomas. *Sci Rep* 2015; **5**: 10169.
16. Zinn KR, Korb M, Samuel S, et al. IND-directed safety and biodistribution study of intravenously injected cetuximab-IRDye800 in cynomolgus macaques. *Mol Imaging Biol* 2015; **17**: 49–57.
17. Day KE, Beck LN, Deep NL, et al. Fluorescently labeled therapeutic antibodies for detection of microscopic melanoma. *Laryngoscope* 2013; **123**: 2681–2689.
18. Day KE, Beck LN, Heath CH, et al. Identification of the optimal therapeutic antibody for fluorescent imaging of cutaneous squamous cell carcinoma. *Cancer Biol Ther* 2013; **14**: 271–277.
19. Day KE, Sweeny L, Kulbersh B, et al. Preclinical comparison of near-infrared-labeled cetuximab and panitumumab for optical imaging of head and neck squamous cell carcinoma. *Mol Imaging Biol* 2013; **15**: 722–729.
20. Friberg S, Mattson S. On the growth rates of human malignant tumors: implications for medical decision making. *J Surg Oncol* 1997; **65**: 284–297.
21. Rosenthal EL, Warram JM, Bland KI, et al. The status of contemporary image-guided modalities in oncologic surgery. *Ann Surg* 2015; **261**: 46–55.